Impaired perceptual learning in a mouse model of Fragile X syndrome is mediated by parvalbumin neuron dysfunction and is reversible.

Anubhuti Goel[1], **Daniel A. Cantu**[1], **Janna Guilfoyle**[3], **Gunvant R. Chaudhari**[1], **Aditi Newadkar**[1], **Barbara Todisco**[1], **Diego de Alba**[1], **Nazim Kourdougli**[1], **Lauren M. Schmitt**[3], **Ernest Pedapati**[3,4], **Craig A. Erickson**[3], and **Carlos Portera-Cailliau**[1,2,*]

[1]Departments of Neurology, David Geffen School of Medicine at UCLA, 710 Westwood Plaza, Los Angeles, CA 90095

[2]Departments of Neurobiology, David Geffen School of Medicine at UCLA, 710 Westwood Plaza, Los Angeles, CA 90095

[3]Department of Psychiatry, Cincinnati Children's Hospital Medical Center, University of Cincinnati College of Medicine

[4]Department of Neurology, Cincinnati Children's Hospital Medical Center, University of Cincinnati College of Medicine

Abstract

To uncover the circuit-level alterations that underlie atypical sensory processing associated with autism, we adopted a symptom-to-circuit approach in the *Fmr1*^{-/-} mouse model of Fragile X syndrome (FXS). Using a go/no-go task and in vivo 2-photon calcium imaging, we find that impaired visual discrimination in *Fmr1*^{-/-} mice correlates with marked deficits in orientation tuning of principal neurons, and a decrease in the activity of parvalbumin (PV) interneurons in primary visual cortex (V1). Restoring visually evoked activity in PV cells in *Fmr1*^{-/-} mice with a chemogenetic (DREADD) strategy was sufficient to rescue their behavioral performance. Strikingly, human subjects with FXS exhibit similar impairments in visual discrimination as *Fmr1*^{-/-} mice. These results suggest that manipulating inhibition may help sensory processing in FXS.

Keywords

autism spectrum disorders; DREADD; Fmr1 knockout, inhibition; layer 2/3; visual cortex

[*]Corresponding author. cpcailliau@mednet.ucla.edu.

Atypical sensory processing, as observed in Fragile X Syndrome (FXS) and across other syndromic and idiopathic forms of autism spectrum disorders (ASD) [1], negatively impacts virtually all activities of daily living. Sensory symptoms are predictive of the subsequent appearance of impaired social behavior and other autistic traits [2, 3]. Thus, a better understanding of the changes in neural circuitry that disrupt perceptual learning could shed light into the mechanistic basis and potential therapeutic avenues for a range of autistic symptoms [2]. FXS is ideally suited to address this issue because it is the leading inherited cause of autism [4], because it lacks major neuroanatomical defects, and because its well-characterized animal model, the *Fmr1*^{-/-} mouse[5], reproduces several aspects of the human disease. *Fmr1*^{-/-} mice not only manifest the immature synaptic defects seen in humans [6, 7], but also multiple symptoms such as anxiety, impaired cognitive flexibility, reduced social interaction, hyperarousal, and sensory over-reactivity [8], that could result from altered sensation. However, at present we lack a clear understanding of how the molecular/synaptic alterations resulting from loss of FMRP affect neuronal networks in ways that can explain specific behavioral features in FXS, such as impaired perceptual learning and discrimination. Furthermore, the lack of directly comparable behavioral paradigms in both humans and animal models also limits the translational potential of discoveries.

Here, we examined impairments of perceptual learning and visual discrimination using a similar behavioral task in mice and humans and then deciphered specific circuit-level disruptions in *Fmr1*^{-/-} mice that bring about the altered behaviors. This parallel "mouse/ human" perspective, derived from a circuit-level understanding of FXS symptoms, is a novel approach to targeting therapeutic interventions. Additionally, although many human psychophysical studies have demonstrated deficits in visual perception in individuals with FXS [9, 10], whether fragile X mice also exhibit similar deficits is not known. We show that *Fmr1*^{-/-} mice exhibit delayed learning of a visual discrimination task and 2-photon calcium imaging in primary visual cortex (V1) revealed that this impairment correlates with reduced numbers and broader tuning of orientation selective pyramidal cells. We also found a reduction in the functional output of parvalbumin (PV) interneurons in V1 of *Fmr1*^{-/-} mice, compared to wild-type (WT) mice. Using an excitatory DREADD approach targeted to PV cells in *Fmr1*^{-/-} mice we could restore their visually evoked responses close to WT levels and this accelerated their rate of learning. By adapting an analogous visual discrimination paradigm for human subjects, we identified a similar deficit in visual discrimination in FXS participants. These findings will help pave the way for new paradigms in targeted treatment development for FXS and ASD.

Results

Fmr1^{-/-} mice exhibit delayed learning on a visual discrimination task

To determine whether *Fmr1*^{-/-} mice manifest perceptual learning deficits associated with abnormal visual sensory discrimination, we trained male and female *Fmr1* knockout (*Fmr1*^{-/-}; n= 21) and wild-type (WT; n= 19) mice (FVB strain) on a go/no-go visual discrimination task [11, 12]. We used separate litters of WT and *Fmr1*^{-/-} mice rather than littermate controls because littermates of different genotypes tend to receive unequal attention from the dam[13] (i.e., the dam neglects the *Fmr1*^{-/-} pups) and this often affects the

health and behavior of *Fmr1*$^{-/-}$ pups, which could bias results. In order to avoid issues with genetic drift, we obtained new WT and *Fmr1*$^{-/-}$ breeders from Jackson Labs at regular intervals (every 1–1.5 years).

Following water deprivation, awake head-restrained young adult mice (2–4 months old) were allowed to run on an air-suspended polystyrene ball while they performed the task (Fig. 1a; see Materials and Methods). Mice were presented with sinusoidal gratings drifting in two orthogonal directions, 45° (preferred, 'go') vs. 135° (non-preferred, 'no-go') at 100% contrast. Incorrect behavioral responses resulted in a 6.5 s 'time-out' period Fig.1b). Task performance, as determined by the discriminability index statistic *d'* (Materials and Methods), was dependent on primary visual cortex (V1), because pharmacological silencing of V1 with bilateral infusions of muscimol, a GABA-A receptor agonist, reversibly disrupted discrimination in WT mice (Fig. 1c).

WT mice learned quickly (3–4 sessions) to lick in response to the preferred orientation for a water reward and withhold licking when presented with the non-preferred orientation (Fig. 1d). In contrast, *Fmr1*$^{-/-}$ mice exhibited a significantly delayed learning curve, compared to the WT mice (Fig. 1d and Supplementary Fig. 1). In addition, we analyzed the behavioral responses over the course of training and found a significant increase in Hit and correct rejection (CR) responses, and a significant decrease in Miss and false alarm (FA) responses, as mice of both genotypes learned the task (Supplementary Fig 2b). *Fmr1*$^{-/-}$ mice exhibited a significantly higher percentage of FA responses compared to WT mice at session 4 (Fig. 1e and Supplementary Fig. 2b), which likely contributed to their poor performance during early training sessions. This increase in FA rates in *Fmr1*$^{-/-}$ mice was not caused by hyperactivity or abnormal locomotion, as the average running speed was similar between genotypes at session 1, or even after the animals reached a d' > 2 (Supplementary Fig. 3). Even though there was no change in running speed in mice of either genotype during the course of each trial on session 1, by session 4, we observed significantly more slowing down in WT than in *Fmr1*$^{-/-}$ mice, towards the end of each trial (Supplementary Fig. 3g-i). However, eventually *Fmr1*$^{-/-}$ mice also learn to slow down for the preferred stimulus at the learned session (Supplementary Fig 3i). Thus, learning of the task is associated with a slowing down in the presence of the preferred stimulus (presumably to consume the water reward)[11].

The delay of *Fmr1*$^{-/-}$ mice in learning the visual discrimination task was evident in female and male mice alike (Supplementary Fig. 4). Importantly, both WT and *Fmr1*$^{-/-}$ mice exhibited significant improvements in task performance throughout training (Fig. 1d). Even though *Fmr1*$^{-/-}$ mice took, on average, 2.5 sessions longer to achieve a d' > 2 (Fig. 1d), there was no significant difference in the final d' values between WT and *Fmr1*$^{-/-}$ mice (Fig. 1f). Thus, *Fmr1*$^{-/-}$ mice eventually achieve the same level of performance in this visual discrimination task as WT controls. Notably, when we reduced the contrast of gratings, *Fmr1*$^{-/-}$ mice did not exhibit obvious impairments in visual discrimination, at least down to 10% contrast (Supplementary Fig. 5), suggesting that their delayed learning was not due to a primary visual deficit.

Impaired performance of *Fmr1*^{-/-} *mice* in a reduced angle task

Fmr1^{-/-} mice are known to exhibit a broadening of receptive fields in somatosensory cortex [14–16]. Similar broader tuning in V1, if it exists, could affect the discrimination of visual stimuli with very similar orientations. Therefore, we next tested whether *Fmr1*^{-/-} mice would be particularly challenged by a reduced angle task, in which the difference in angle between the preferred and non-preferred orientation was gradually reduced to 7.5°, after the animals had learned the basic 90° task (Fig. 2a). Mice that had already maintained an expert-level performance (d' > 2) on the 90° task were tested for only two sessions at each of the reduced angle tasks (starting at 15°, then 10° and finally 7.5°). The d' values shown in Fig. 2b are averages of those two sessions. Overall, there was a significant decrease in performance across both genotypes when the angle between the orientations was gradually reduced. However, changes in d' at different angles suggest that the threshold for discrimination for WT mice was at or below 7.5°, whereas as it was 15° for *Fmr1*^{-/-} mice (Fig. 2b).

To further probe the extent to which mice were challenged by this reduced angle task, we assessed their response times and observed a significant delay in the distribution of licking onset in *Fmr1*^{-/-} mice, compared to WT mice, for the reduced angle task, but not for the normal (90°) task (Fig. 2c). This suggests that *Fmr1*^{-/-} mice take longer to make a decision only in the face of ambiguous sensory information.

Orientation tuning deficits in V1 correlate with task performance in *Fmr1*^{-/-} mice

Having established a defect in perceptual learning in the fragile X mouse model that is relevant to the human disease, we next adopted a reverse engineering approach to identify the circuit- and neuronal-level alterations that might underlie the impaired visual discrimination. In light of various reports of cortical hyperexcitability and network hypersynchrony in *Fmr1*^{-/-} mice [6, 17, 18], we first investigated whether the perceptual learning deficit we observed in *Fmr1*^{-/-} mice, was caused by abnormal orientation tuning of pyramidal cells in V1. To test this, we performed in vivo 2-photon calcium imaging in layer (L) 2/3 neurons in awake mice running on a floating polystyrene ball (Fig. 3a-c; Materials and methods). A rAAV to express GCaMP6s [19] was injected in V1 following stereotaxic coordinates, and successful targeting was confirmed using intrinsic signal imaging (Fig. 3b). We recorded both spontaneous and visually evoked activity from L2/3 neurons in mice that were fully acclimated to the experimental rig and running vigorously throughout the calcium imaging session (Fig. 3c). For the latter, WT and *Fmr1*^{-/-} mice (n= 9 and 10, respectively) were presented with four sequential presentations of sinusoidal gratings drifting in 8 different directions (4 orientations), at random (Fig. 3d; Materials and methods). Although previous studies have reported hyperexcitable cortical circuits in *Fmr1*^{-/-} mice (reviewed in [6]), we did not observe a significant increase in either spontaneous or visually evoked activity in *Fmr1*^{-/-} mice (Fig. 3e and Supplementary Fig. 6a, b).

Despite the seemingly normal frequency of visually evoked activity in *Fmr1*^{-/-} mice, mutant mice had a significantly lower percentage of orientation selective (OS) cells in L2/3 (Fig. 3f). Importantly, when we trained these mice on the visual discrimination task, we found a significant inverse correlation between the percentage of OS cells and the number of days it took animals to reach a d' > 2 (Fig. 3g). This implies that, with fewer available OS cells in

V1, *Fmr1*^{-/-} mice had more difficulty discriminating between two different orientations, particularly when the difference was small (Fig. 2 a-c). In addition, in vivo calcium imaging revealed that L2/3 neurons in V1 of *Fmr1*^{-/-} mice had a significantly broader tuning compared to those in WT mice (Fig. 3h). This 6.6° difference in the mean tuning width of pyramidal neurons in V1 between WT and *Fmr1*^{-/-} mice, though slight, might be sufficient to explain why *Fmr1*^{-/-} mice can discriminate at 15° but not at 10°. Additionally, we found a significant correlation between the tuning width of L2/3 cells and the number of days it took the animals to reach a d' > 2 (Supplementary Fig. 7), which suggests that the broader tuning of the pyramidal neurons in V1 contributes to the delayed learning in *Fmr1*^{-/-} mice.

Reduced activity of parvalbumin cells in V1 in *Fmr1*^{-/-} mice

Abnormal V1 network dynamics pertaining to orientation selectivity and tuning width could be the result of dysfunction in parvalbumin (PV) interneurons, the most prevalent inhibitory neuron in V1 [20]. PV cells exhibit very broad orientation tuning by simply responding to all orientations, since they receive local input from a wide range of orientation tuned pyramidal cells [21–23]. Furthermore, selective stimulation of PV cells in V1 with channelrhodopsin-2 leads to improved feature selectivity and visual discrimination [12]. For these reasons, we tested the hypothesis that PV cells were hypoactive in fragile X mice. We used in vivo calcium imaging to record the activity of PV neurons in V1 of WT and *Fmr1*^{-/-} mice (n= 6 and 7, respectively) that expressed Td-Tomato in PV neurons (PV-Cre mice × ai9 mice; see Materials and methods). At the time of the cranial window surgery, we injected a Cre-dependent virus into V1, to selectively express GCaMP6s in PV cells (Fig. 4a, b). Our calcium imaging recordings revealed stark differences in the activity of PV cells between WT and *Fmr1*^{-/-} mice; whereas traces of PV cell activity in WT mice showed the expected broadly tuned, non-selective responses to visual stimuli, traces of PV cells in *Fmr1*^{-/-} mice exhibited reduced visually evoked activity (Fig. 4c). (Fig. 4d), *Fmr1*^{-/-} mice exhibited a significantly lower frequency of calcium peaks (see Methods) triggered by visual stimuli (Fig. 4d, 4e). One of our criteria for selecting PV cells for analysis in both WT and *Fmr1*^{-/-} mice was that they exhibit at least one calcium transient in the recordings (Materials and methods), and neither the proportion of active PV cells (Fig. 4f), nor the amplitude or frequency of spontaneous calcium transients in PV cells, were significantly different between WT and *Fmr1*^{-/-} mice (Supplementary Fig. 8). We also found a significantly lower fraction of stimulus-responsive PV cells in *Fmr1*^{-/-} mice (Fig. 4g), which would also ultimately be expected to affect the functional output of V1.

A DREADD strategy that restores PV cell activity and orientation tuning in V1 accelerates learning of the visual task in *Fmr1*^{-/-} mice.

Based on the finding that PV cells were indeed hypoactive in *Fmr1*^{-/-} mice, we hypothesized that a successful manipulation of PV cell activity that would restore their output in these animals, might also improve their performance on the visual discrimination task. Hence, we used a Designer Receptors Exclusively Activated by Designer Drugs (DREADD) approach [24] (see Materials and methods) to selectively express the excitatory hM3Dq receptor in PV cells of *Fmr1*^{-/-} mice (n= 6; Fig. 5a). We then used the hM3Dq ligand, clozapine-N-oxide (CNO, 5 mg/kg, i.p.), to excite PV cells and increase their output in these *Fmr1*[-/-, hM3Dq] mice. Overexpressing hM3Dq in PV cells alone (before administering CNO) did not affect

visually evoked activity of PV cells in *Fmr1*^{-/-, hM3Dq} mice (Supplementary Fig. 9a-d). In contrast, 30 min after a single CNO injection, we observed a robust increase in visually evoked PV cell output in these *Fmr1*^{-/-, hM3Dq} mice (Fig. 5 b-e). Specifically, we observed a significant increase in both the frequency of visually evoked calcium transients in PV cells of *Fmr1*^{-/-, hM3Dq} mice (Fig. 5c), and in the frequency of individual peaks of activity (Fig. 5d). Spontaneous activity was unaffected by CNO (Supplementary Fig. 10). The fraction of stimulus responsive PV cells in *Fmr1*^{-/-, hM3Dq} mice was also significantly increased by CNO, restoring it to WT levels (Fig. 5e). Importantly, the fact that we could increase the activity of PV cells with DREADDs supports the notion that PV cells were not silent in *Fmr1*^{-/-} mice due to poor health. Also, the proportion of PV cells that was active did not change after CNO administration (not shown), suggesting that the DREADD effect on the fraction of visually responsive PV neurons was not due to simply making previously silent cells more active.

Having restored visually evoked PV cell activity in *Fmr1*^{-/-/, hM3Dq} mice to near normal WT levels, we hypothesized that we might be able to reverse the delay in learning the visual discrimination task. A subset of the DREADD-expressing *Fmr1*^{-/-} mice were therefore trained on the standard visual discrimination task (90° angle) and injected with CNO, ~30 min prior to each training session. This chemogenetic manipulation resulted in a leftward shift in the learning curve (i.e., faster learning) of CNO-treated *Fmr1*^{-/-, hM3Dq} mice (Fig. 5f), indicating that we were able to rescue the learning impairment by acutely elevating the PV cell output. CNO led to a significant reduction in the number of days required to reach expert level (d' > 2) on the visual discrimination task compared to *Fmr1*^{-/-} mice (Fig. 5g). Interestingly, the rate of FA responses in these CNO-treated *Fmr1*^{-/-, hM3Dq} mice was similar to that of WT mice (not shown). Importantly, injection of CNO alone in the absence of DREADDs in *Fmr1*^{-/-}, did not rescue behavior (Fig. 5g). To come full circle back to OS cells in V1, we also tested whether the DREADD manipulation on PV cells would be sufficient to affect the properties of pyramidal neurons in the circuit. Calcium imaging with rAAV-GCaMP6s in a group of *Fmr1*^{-/-, hM3Dq} mice revealed that CNO administration significantly raised the proportion of orientation selective pyramidal cells and showed a trend towards sharper tuning (Fig. 5h, i). Notably, the relationship between PV cell output and behavior was apparent from the negative correlation between the fraction of stimulus responsive PV cells and the number of days needed to reach a d' > 2 (Supplementary Fig. 11). This relationship showed clearly how *Fmr1*^{-/-, hM3Dq} mice treated with CNO were not distinguishable from WT mice.

Fragile X patients exhibit similar defects in visual discrimination as *Fmr1*^{-/-} mice

It was recently argued that the absence of directly comparable behavior paradigms between human and animal studies is an impediment to progress in translational research for autism and its associated genetic disorders [2]. It might even explain, in part, the failure of clinical trials in FXS [25]. In order to assess the translational potential of our findings of impaired visual discrimination (and, by extension, the associated circuit dysfunction) in *Fmr1*^{-/-} mice, we next asked whether the same perceptual learning task could be applied to humans with FXS. We implemented the same paradigm as in mice with relatively minor modifications, to make it suitable for individuals with FXS (Fig. 6a, b; Materials and methods). Healthy

control human participants and FXS participants (n= 8 each; see Supplementary Tables 1 and 2) were administered the task. Most individuals affected by FXS could complete the task at 90° but demonstrated on average a significantly lower d' than heathy controls (Fig. 6c). Performance declined slightly in some healthy control participants at reduced angles, but on average, this was not significant. In contrast, FXS participants showed a clear trend towards a lower d' on the 15° task compared with 90° or 45° tasks (p= 0.06). Additionally, the performance of FXS participants was lower than that of controls for all the angles measured. Thus, FXS participants and *Fmr1*^{-/-} mice exhibit strikingly similar visual discrimination deficits for ambiguous stimuli of similar orientations. This suggests that a discrimination task like the one we used could eventually be used as a biologically based outcome measure of sensory processing in human clinical trials.

DISCUSSION

Progress in FXS research is limited by the lack of clearly identified circuit-level alterations that can explain the neuropsychiatric phenotype that characterizes the disorder. Though circuit activity in monogenetic murine models of autism can be readily interrogated and manipulated, there is increasing interest to demonstrate both face validity and predictive validity for these translational approaches to be used in clinical trials [2]. To bridge this gap, we implemented a fully translatable behavioral assay of perceptual learning and discrimination in both *Fmr1*^{-/-} mice and FXS patients, and followed a symptom-to-circuit approach to delineate specific circuit-level defects using calcium imaging in V1. Our discovery that *Fmr1*^{-/-} mice have a reduced proportion of orientation selective neurons in V1, and these cells have abnormally broad tuning, as well as extremely hypoactive PV cells, provides a circuit mechanism of their behavioral deficits on this task. The fact that we could rescue the perceptual deficits in mice by restoring activity in PV cells with DREADDs and that humans with FXS exhibit analogous deficits in visual discrimination, provides a realistic path for novel translational clinical trials.

Our data implicates a role for PV cells in circuit dysfunction in FXS through converging evidence of their hypoactivity from experiments in two different groups of mice (*Fmr1*^{-/-} and *Fmr1*[-/-, *hM3Dq*]), and from the DREADD approach, which not only restored PV cell activity, but also raised the percentage of orientation selective pyramidal cells in V1. But additional studies will be necessary to fully elucidate the role of PV cells in network dysfunction in FXS, at least in part because their influence on the circuit is rather complex and likely depends on the level and duration of their engagement in a given computation [26]. Moreover, it is also possible that suppressed activity of PV neurons might paradoxically lead to an increase in inhibitory synaptic input to L2/3 ("network suppression) as recently described in auditory cortex [27].

It is exciting to consider that PV cell dysfunction could be involved in other aspects of FXS, such as impaired neuronal adaptation in tactile defensiveness [8]. Additionally, by rapidly translating this paradigm into a clinical population, we have substantially reduced potential barriers to further study whether PV cell dysfunction represents an important aspect (or even the principal one) of a *canonical micro-circuitry* that may generalize to other forms of ASD [2]. In the future, our pilot human FXS data will need to be bolstered by studies that

incorporate visual evoked potentials to clarify the relationship between sensory processing deficits in the visual pathway and impaired perceptual learning[28, 29].

Running is known to have an impact on visually evoked activity of both excitatory and inhibitory neurons in V1 [30–32]. Nevertheless, because we did not observe any differences in the magnitude of running between genotypes, we cannot attribute the deficits of $Fmr1^{-/-}$ mice in visual discrimination, or their altered network activity, to any differences in locomotion.

The lack of changes in spontaneous neuronal activity in V1 of $Fmr1^{-/-}$ mice, together with the fact that we could manipulate the gain of PV cell output to restore circuit function and rescue behavior, highlights the important notion that perhaps the basal circuit connectivity remains 'intact' in adult $Fmr1^{-/-}$ mice. However, depending on the computational demands imposed by sensory environment, $Fmr1^{-/-}$ mice (and by inference humans with FXS) may exhibit subtle functional alterations in cortical circuits that render them unable to efficiently process sensory information in ways that impair their ability to properly utilize this information to learn perceptual tasks or adequately discriminate between similar sensory stimuli. For example one simple interpretation of our findings is that perhaps manipulating orientation tuning in FXS could improve visually guided behaviors that are critical for playing sports, driving or judging emotions. In conclusion, our study offers hope that simple therapeutic strategies that target relevant relatively subtle circuit defects may be of value in treating specific behavioral impairments in FXS.

Online Methods

Experimental animals

All experiments followed the U.S. National Institutes of Health guidelines for animal research, under an animal use protocol (ARC #2007–035) approved by the Chancellor's Animal Research Committee and Office for Animal Research Oversight at the University of California, Los Angeles. Experiments in Figs. 1 and 2 used male and female FVB.129P2 WT mice (JAX line 004828) and $Fmr1^{-/-}$ mice [5] (JAX line 004624) and experiments in Fig. 3 used male and female PV-Cre mice (JAX line 008069) that were crossed to the Ai9 (Td-Tom) reporter line (JAX line 007909) and the resulting PV-Cre × Ai9 mice were back crossed to FVB WT and $Fmr1^{-/-}$ mice for 8 generations. All mice were housed in a vivarium with a 12/12 h light/dark cycle and experiments were performed during the light cycle. The FVB background was chosen because of its robust breeding, because FVB $Fmr1^{-/-}$ dams are less prone to cannibalizing their pups, and because FVB $Fmr1^{-/-}$ mice have well-documented deficits in sensory processing[6]. Additionally, to improve the survival of $Fmr1^{-/-}$ pups due to the possibility of littermates with different genotypes receiving unequal attention from the dam[13] we used homozygous litters.

Go/No-go visual discrimination task for head-restrained mice—Awake, head-restrained young adult mice (2–4 months) were allowed to run on an air-suspended polystyrene ball while they were trained on the visual discrimination paradigm. Prior to performing the discrimination task the animals were subjected to handling, habituation and pretrial (Fig. 1a). After recovery from headbar/cranial window surgery, mice were handled

gently for 5 min every day, until they were comfortable with the experimenter and would willingly transfer from one hand to the other to eat sunflower seeds. This was followed by water deprivation (giving mice a rationed supply of water once per day) and habituation to the behavior rig. During habituation, mice were head-restrained and acclimated to the enclosed sound-proof chamber and allowed to run freely on the 8 cm polystyrene ball (Fig. 1b). Eventually, mice were introduced to the visual stimuli on the screen and the lickport (either commercial from Island Motion or custom-built at the UCLA electronics shop) that dispensed water (3–4 μL). This was repeated for 15 min per session for 2–3 days. Starting water deprivation prior to pretrials motivated the mice to lick[33]. After habituation and ~15% weight loss, mice started the pretrial phase of the training. During pretrials, drifting sinusoidal gratings at 8 different directions were displayed on the screen. The monitor was placed at a distance of 20 cm from the mouse and stimuli were presented at random for 3 s, and each stimulus was coupled with a water reward dispensed through a lickport at 2 s after stimulus presentation. The mice were required to learn to associate a water reward soon after the stimulus was presented on the screen and that there was no water reward in the inter-trial interval (3 s period between trials). Initially, during pre-trials the experimenter pipetted small drops of water onto to the lickport to coax the mice to lick. Once the mice learned this and licked with 85% efficiency, they were advanced to the go/no-go task. We found no significant difference in the pretrial training period between *Fmr1*^{-/-} and WT mice (WT: 5.6 ± 0.3 d; *Fmr1*^{-/-}: 5.1 ± 0.5 d; p= 0.4, t-test).

During the go/no-go visual discrimination task, drifting sinusoidal gratings (temporal frequency of 2 Hz, spatial frequency of 0.01 cycles /degree and 100% contrast) were displayed on a computer monitor (21" display) for 3 s, with water reward occurring 2 s after stimulus onset. Sinusoidal gratings of 45° and 135° orientations were randomly presented on the screen, but only the 45° orientation was coupled with a water reward (Fig. 1c). Mice learned to discriminate between the two orientations and to lick in anticipation of the water reward during the 45° presentation (i.e., 'go') while withholding licking during the 135° orientation (i.e., 'no-go'). Licking was recorded during the entire 3 s period; hence, the lick onset time in Fig. 2c is from the start of stimulus; however, only licking between 2 s and 3 s contributed to the calculation of the behavioral response. Depending on the stimulus presented, the animal's behavioral response was characterized as "Hit", "Miss", "Correct Rejection" (CR) or "False Alarm" (FA) (Fig. 1c). An incorrect response resulted in a time-out period of 6.5 s, where nothing is presented on the screen. Training sessions consisted of 350 trials. To examine the psychometric threshold of task performance was tested at different contrasts (Supplementary Fig. 5). d' (discriminability index) was calculated as:

$$dprime = norminv(fraction\ of\ Hits) - norminv\ (fraction\ of\ FAs)$$

Norminv is a MATLAB function that returns the inverse of the normal cumulative distribution function.

Custom-written routines and Psychtoolbox in MATLAB were used to present the visual stimuli, to trigger the lickport to dispense water, and to acquire data.

Five *Fmr1$^{-/-}$* mice and 1 WT mouse were excluded from the data because the mice lost > 25% body weight (a criterion we established a priori). This had adverse effects on their health that was manifested in listlessness, reduced grooming and interaction with cage mates and, occasionally, seizures.

Mouse locomotion video acquisition and analysis—Evenly distributed dots (1 cm in diameter) were painted on the surface of the polystyrene ball (Fig. 1b) to capture its motion with a high-speed webcam (Logitech C920). Custom MATLAB routines were used to analyze the ball motion videos. The webcam acquired 720×1280 videos at 60 fps. We ran each frame through a Hough transform to identify dark circles in the image (Supplementary Fig. 3). A series of spatial filters excluded irrelevant circles that were outside the ball's circumference. A cap of 200 cm/s was set as a threshold above which there was a significant motion blur that led to inconsistent speed calculations. The algorithm for calculating ball motion speed first identified all the dots on the ball visible in each frame of the video, using spatial filters to isolate circular dots only on the ball. Then, it compared consecutive frames to determine how much each dot had moved relative to its position in the previous frame. Finally, the algorithm calculates the distance that dots moved and the median of overall dot movement over a 0.1 s interval to output absolute velocity of the ball. The distance the dot moved was computed as a linear representation of the projection of the dot onto the camera's detector surface. Due to our segmentation, most dots we tracked were close to the center of the circle we projected onto the ball, so this straight-line representation was a fairly good approximation of the true rotational speed of the ball A separate script then aligned the velocities to the different stimulus presentations, which allowed us to compare mouse speeds at different points during the trial.

Bilateral cannula implantation surgery—Similar to the cranial window surgery, adult WT mice were anesthetized with isoflurane and secured to a stereotaxic frame. We placed the mice on a heating blanket and used artificial tears to keep their eyes moist throughout the surgery. After exposing the skull, we drilled two shallow burr holes targeting V1 on both hemispheres (−4.0 mm posterior and +/− 2.8 mm lateral to Bregma). We then inserted 22 G guide cannulas (Plastics One) into the holes to a depth of −0.4 mm below the dura and the internal cannula projected further to −0.6 mm. After securing the cannula using cyanoacrylate glue (Krazy Glue) that was accelerated with cyanoacrylate glue accelerator (Insta-Set), dummy cannulas were screwed on to ensure that the guide cannula did not get clogged. Finally, we attached a headbar that would be used to immobilize the animal's head during the visual behavior task. The cannula pedestals and headbars were further secured using dental cement that covered all exposed parts of the skull. After recovery, mice completed the visual discrimination task. Once the mice reached a d' > 2, 8 μL (Sigma-Aldrich) solution (1 mg/ml in water) was infused bilaterally in isoflurane anesthetized mice through a 28 G internal (C313IS, Plastics One) and 22 G guide (C313GS, Plastics One) cannula. After full recovery from anesthesia (<15 min), mice were immediately re-tested on the visual discrimination task. Two mice were also re-tested the following day to evaluate task performance after washout of muscimol. To confirm the correct targeting of the cannulas and muscimol infusions, mice were also infused by the fluorescent dye DiI

(V2285, Thermo Fisher) followed by transcardial perfusion with paraformaldehyde and histology (see below).

Viral constructs—AAV1.Syn.GCaMP6s.WPRE.SV40 and AAV1.Syn.Flex.GCaMP6s.WPRE.SV40 were purchased from the University of Pennsylvania Vector Core and diluted to a working titer of $2e^{13}$ or $2e^{12}$ (to enable a longer period of optimal expression) with 1% filtered Fast Green FCF dye (Fisher Scientific). GCaMP6s was chosen over GCaMP6f because it detects more active neurons and it has an improved signal-to-noise ratio for more reliable detection of single action potentials during sparse spontaneous activity [19]. For DREADD experiments, pAAV.hSyn.DIO.hM3D(Gq).mCherry was purchased from Addgene and diluted to a working titer of $2e^{12}$ with 1% Fast Green FCF dye.

Cranial window surgery—Experiments were started with craniotomies performed at 6–8 weeks on the four different mouse lines mentioned above. Mice were anesthetized with isoflurane (5% induction, 1.5–2% maintenance via a nose cone) and placed in a stereotaxic frame. A 4.5 mm diameter craniotomy was performed over the right primary visual cortex (V1) and covered with a 5 mm glass coverslip, as previously described [34, 35]. Before securing the cranial window with a coverslip, we injected ~50 nl of AAV1.Syn.GCaMP6s.WPRE.SV40 (Fig. 3a, in vivo calcium imaging of L2/3 pyramidal neurons), or a mixture of AAV1.Syn.GCaMP6s.WPRE.SV40 and AAV1.Syn.Flex.GCaMP6s.WPRE.SV40 (Fig. 4, *in vivo* calcium imaging in PV cells), or a cocktail of AAV1.Syn.Flex.GCaMP6s.WPRE.SV40 and pAAV.hSyn.DIO.hM3D(Gq).mCherry (Fig. 5, to activate PV cells with DREADDs). A custom U-shaped aluminum bar was attached to the skull with dental cement to head restrain the animal during behavior and calcium imaging.

Optical intrinsic signal (OIS) imaging—Two weeks after cranial window surgery, OIS imaging was used to map the location of V1. Visual stimulation was provided by a piezo-actuator (Physik Instrumente) that deflected light from a red light emitting diode in front of the contralateral eye. The response for 30 stimulation trials was averaged, each consisting of 100 Hz deflections for 1.5 s. The response signal divided by the averaged baseline signal, summed for all trials, was used to generate the visual cortical map.

***In vivo* two-photon calcium imaging**—Calcium imaging was performed on a custom-built 2-photon microscope, with a Chameleon Ultra II Ti:sapphire laser (Coherent), resonant scanning mirrors (Cambridge Technologies), a 25× objective (1.05 NA, Olympus), multialkali photmultiplier tubes (R3896, Hamamatsu) and ScanImage software [36]. Prior to calcium imaging, head-restrained mice were habituated to a sound-proof chamber and allowed to run freely on a polystyrene ball (Fig. 1b). Eventually, mice were introduced to the visual stimuli on the screen. This habituation phase lasted 3–4 sessions and there was no difference between genotypes in the time of habituation. Visual stimuli were generated using custom-written MATLAB (Mathworks) routines using Psychtoolbox that consisted of full-field square wave drifting gratings (2 cycles/s, 0.005 spatial frequency, 32 random repeats of 8 orientations) presented for 3 s and separated by a 3 s-long grey screen. Both spontaneous

and visually evoked responses of L2/3 pyramidal cells from V1 were recorded at 15 Hz in 2–4 fields of view. Each FOV consisted of a median of 63 pyramidal cells (range: WT= 54–81; $Fmr1^{-/-}$ = 57–79) or 8 PV cells (range: WT= 3–10; $Fmr1^{-/-}$= 3–8). In each animal, imaging was performed at 2–3 depths (150–250 μm), and data was averaged from movies collected across all FOVs.

Data analysis for calcium imaging—Calcium-imaging data were analyzed using custom-written MATLAB routines, which included modifications of our previously described MATLAB code[17]. This code is available from the corresponding author upon request. X-Y drift in the movies was corrected using an iterative, cross-correlation-based, non-rigid alignment algorithm[37]. A semi-automated algorithm[19] was used to select regions of interest (ROIs), each representing a single cell body, and to extract the fluorescence signal (*F*) for each ROI. A "modified Z-score" $Z_f(t)$ vector for each neuron was calculated as:

$$Z_f(t) = \frac{F(t) - mean(baseline)}{std(baseline)}$$

where the baseline period is the 10 s period with the lowest variation (standard deviation) in F/F[8]. All subsequent analyses were performed using the $Z_f(t)$ vectors.

Neuropil subtraction was performed by removing the local fluorescence signal surrounding each ROI[18]. Peaks of activity were then detected in the Z-scores using the PeakFinder MATLAB script. These peaks were used to calculate the mean Z-score fluorescence (an estimate of amplitude of the fluorescence signal) and the frequency of events. To remove any bias resulting from peak detection, especially in PV cells, we also calculated the frequency of events based on the magnitude of the fluorescence signal ('area under the curve'). For this analysis, we calculated the area under the curve for each fluorescence trace and divided that by the number of frames during which a stimulus is presented (i.e., 15 frames or 3s). This was then multiplied by the frame rate to get a Z-score of fluorescence per second.

Orientation selective cells were defined by an orientation selectivity index (OSI) calculated as

$$OSI = \frac{(Z_{pref} - Z_{orth})}{(Z_{pref} + Z_{orth})}$$

where Z_{orth} is the mean response to the orientation orthogonal to the preferred one (Z_{pref})[38]. A cell was considered orientation-selective if it had an OSI ≥ 0.5.

To quantify visually evoked activity, we averaged the responses of neurons during the 3 s of drifting gratings stimulation and the 3 s of gray screen that followed the visual stimulus. To quantify spontaneous activity, we conducted separate recordings during which the animals were presented a static gray screen. In order to determine whether an individual cell showed a time-locked or stimulus selective response to a visual stimulus in Fig. 3 and Supplementary Fig. 9c (which examines the correlation between the stimulus and the fluorescence signal in PV cells), we used a probabilistic bootstrapping method as described

previously [8]. First, we calculated the correlation between the stimulus time-course and the Z_F vector, followed by correlation calculations between the stimulus time-course and 1,000 scrambles of all calcium activity epochs in Z_F (epoch = consecutive frames wherein Z_F 3). The 1,000 comparisons generated a distribution of correlations (R values), within which the correlation of the unscrambled data and the stimulus fell at any given percentile. If the calculated percentile for a cell was less than 1%, then we described that cell as being stimulus selective. Correlations in Figs. 3g, 5j and Supplementary Fig. 7 were calculated using a Pearson's correlation.

Our tuning width calculation procedures are similar to what has been described before [39]. First, we generate a tuning curve of the mean Z-score values of the responses for each orientation presented. The orientation with the largest mean response is determined to be the preferred orientation. A Gaussian is then fitted to the tuning curve and the tuning width is determined to be the width at half the maximum value of the fitted Gaussian. The equation of the Gaussian we use is the same as in Akerboom et al.

$$\sigma \cdot \sqrt{2 \cdot \ln 2}$$

We included only neurons that elicited at least one calcium transient during the duration of the recording; neurons were excluded if they were deemed inactive on the basis of calcium imaging data (Pyramidal neurons excluded: WT= 0.1%; $Fmr1^{-/-}$= 0.1%. PV neurons excluded: WT= 0.1%; $Fmr1^{-/-}$= 0.1%).

Transcardial perfusion, Dil histology—Mice were deeply anesthetized with isoflurane and underwent transcardial perfusion with 4% paraformaldehyde solution in sodium phosphate buffer (composition in mM: 30 mM NaH_2PO_4, 120 mM Na_2HPO_4, pH 7.4). Brains were kept overnight at 4°C first in 4% paraformaldehyde solution (pH 7.4) and then stored in 30% sucrose (in phosphate buffered saline at 4°C until sectioned.

Human subjects—Eight males with FXS and eight male healthy controls, matched on chronological age, completed the visual discrimination experiment (Table S1). Testing was conducted at a regional academic pediatric medical center where the participants with FXS were originally recruited as part of our Center for Collaborative Research in Fragile X (U54). Approval of this study was granted through the Institutional Review Board at Cincinnati Children's Hospital Medical Center. All participants >18 years of age provided written consent and minors provided assent, as well as written consent from their legal guardians. Additional consent was obtained to use the de-identified photograph of a FXS participant performing the task. All FXS participants had full FMR1 mutations (>200 CGG repeats) confirmed by genetic testing. No participants had a history of non-febrile seizures or treatment with an anticonvulsant medication (Table S2). FXS participants completed the Abbreviated Battery of the Stanford-Binet Intelligence Scales-Fifth Edition (SB-5). Control participants were recruited through hospital-wide and community advertisements and were excluded for a history of developmental or learning disorders or significant psychiatric disorder (e.g., schizophrenia) in themselves or first degree-relatives, or for a family history

of ASD in first- or second-degree relatives based on a brief screening interview. All study procedures were approved by the local Institutional Review Board.

Human FXS and control participants completed a visual discrimination task that was analogous to that used with mice with relatively minor modifications. Due to the additional cognitive demands of a go/no-go paradigm, including inhibitory control, which is known to be impaired in FXS [40], we designed a forced two-choice visual discrimination task, so that all FXS participants could learn and perform the task in a single session. It is conceivable, however, that FXS subjects could have learned the go/no-go task with subsequent training sessions, just as the mice required consecutive sessions to learn; however, time constraints and burden on the patient population limited our ability to do so. Visual gratings were displayed on a 13-inch Hewlett Packard laptop computer with a 15-inch liquid crystal display and made responses on designated keys on the laptop keyboard. During the task, when the visual grating appeared to move from right side to left side, subjects were instructed to press the corresponding left-sided key ('Z' or 'A'), and when the visual grating appeared to move from left to right, subjects were instructed to press the corresponding right-sided key ('L' or 'M'). If participants correctly responded to the direction of the stimulus, they received positive visual feedback (e.g., images of popular video game cartoon characters were displayed on the computer screen). If participants incorrectly responded to the direction of the stimulus, they received negative visual feedback (e.g., a large red 'X' was displayed). Visual gratings appeared on screen for 4 s, during which participants could respond. Once the participant responded or at the end of 4 s, feedback was presented for 1 second. The following trial would begin 3 s later. All participants completed the first-order visual task, followed immediately by the second-order visual task. For each of the tasks, visual gratings appeared in four blocks of 30 trials, each block consisted of one condition: 180/0, 45/90, 67.5/45, 82.5/15 degrees. The order of the blocks was presented randomly, but participants always received first-order prior to second-order. Prior to administration of the task, participants completed two practice blocks. During the first practice block, a smiley face emoji moved from left to right on the screen (or right to left), and participants were instructed to press the corresponding key based on the direction the smiley faced moved. In the second block, visual gratings at 50/80 angle were presented, and participants pressed key corresponding to direction of movement. Twelve trials of each practice block were administered. If participants did not reach 50% correct trials, the block was repeated one time for a total of 24 trials per block. All participants met practice criterion. Depending on the stimulus presented, the subject's behavioral response was characterized as "Right (similar to Hit)", "NR (no response)" or "Wrong (similar to FA)". Since this was a forced two-choice visual discrimination task, a modified d' (discriminability index) was calculated as follows:

$$dprime = Norminv\,(fraction\ of\ Rights) \ - \ norminv\,(fraction\ of\ Wrongs)$$

Statistical analyses—Statistical analysis of normality (Lilliefors and Shapiro Wilk tests) were performed on each data set and depending on whether the data significantly deviated from normality ($p<0.05$) or did not deviate from normality ($p>0.05$) appropriate non-parametric or parametric tests were performed. The statistical tests performed are mentioned

in the text and the legends. For parametric two-group analyses, a Student t-test (paired or unpaired) was used. For non-parametric tests, we used the following: Mann-Whitney test (two groups), Kruskal-Wallis test (three or more groups) and the Friedman test (repeated measures). In the figures, significance levels are represented with the following convention: * for $p<0.05$; ** for $p<0.01$, *** for $p<0.005$.

In all the figures, we plot the standard error of the mean (s.e.m.). Graphs either show individual data points from each animal or group means (averaged over different mice) superimposed on individual data points.

Sample size—We did not use statistical methods to predetermine sample sizes. For all the main results shown in Figures 1–3 we used sample size =>10 mice and subsequent statistics were performed using number of mice as sample size. Working with $Fmr1^{-/-}$ can be technically challenging for several reasons: 1) Fmr1-/- mothers have a higher incidence of cannibalization, 2) $Fmr1^{-/-}$ mice can require extra handling in order to habituate them to any behavioral task and extra care is required during water deprivation because a fraction of them can show adverse effects such as excessive weight loss, which could lead to seizures. Hence to maintain feasibility of experiments and ethical use of numbers of animals for most of our experiments we used at least 10 mice per group.

In Fig 4 and 5 we used triple transgenic mice where PV-Cre mice were crossed with Ai9 mice and these were then back crossed to FVB WT and $Fmr1^{-/-}$ mice for 8 generations. Generation of a triple transgenic line was time consuming and resource intensive, and we faced the same technical challenges associated with using $Fmr1^{-/-}$ mice; hence, we used n => 6 mice. Again statistics were performed using the number of mice as the sample size.

The sample size we used is consistent with previously published studies [11, 41]. For the inactivation of visual cortex experiments (Fig 1c) the sample size was in agreement with previous studies.[42, 43]

For Fig. 6 we used n=8 humans for each group. Recruiting age and gender matched Fragile X patients is challenging, however a sample of 8 is comparable to the number of human subjects used in previously published studies.[44, 45]

Randomization—We ensured that during a behavior training cycle both WT and $Fmr1^{-/-}$ were included to exclude any biases introduced by experimenters or the training rig. Similarly on a particular testing day Fragile-X subjects were randomized with control subjects.

Blinding—G.C., A. N., B.T., D.A. were blinded to the genotype in a 60% of mice used in all the experiments during visual discrimination training.

Reporting Summary—Further information on experimental design is available in the Life Sciences Reporting Summary linked to this article.

Data availability—All the analyzed data reported in this study is available from the corresponding author upon request.

Code availability—All code used in this manuscript is available from the corresponding author upon request.

Supplementary Material

Refer to Web version on PubMed Central for supplementary material.

ACKNOWLEDGEMENTS

REFERENCES

1. Association A.P. Diagnostic and Statistical Manual of Mental Disorders (DSM−5), Edn. 5th (2013).

2. Robertson CE & Baron-Cohen S Sensory perception in autism. Nat Rev Neurosci 18, 671–684 (2017). [PubMed: 28951611]

3. Estes A et al. Behavioral, cognitive, and adaptive development in infants with autism spectrum disorder in the first 2 years of life. J Neurodev Disord 7, 24 (2015). [PubMed: 26203305]

4. Rife M et al. Incidence of fragile X in 5,000 consecutive newborn males. Genet Test 7, 339–343 (2003). [PubMed: 15000813]

5. Dutch-Belgian Fragile X Consortium Fmr1 knockout mice: a model to study fragile X mental retardation. Cell 78, 23–33 (1994). [PubMed: 8033209]

6. Contractor A, Klyachko VA & Portera-Cailliau C Altered Neuronal and Circuit Excitability in Fragile X Syndrome. Neuron 87, 699–715 (2015). [PubMed: 26291156]

7. He C & Portera-Cailliau C The trouble with spines in fragile X syndrome: density, maturity and plasticity. Neuroscience in press (2012).

8. He CX et al. Tactile Defensiveness and Impaired Adaptation of Neuronal Activity in the Fmr1 Knock-Out Mouse Model of Autism. J Neurosci 37, 6475–6487 (2017). [PubMed: 28607173]

9. Farzin F, Whitney D, Hagerman RJ & Rivera SM Contrast detection in infants with fragile X syndrome. Vision Res 48, 1471–1478 (2008). [PubMed: 18457856]

10. Kogan CS et al. Differential impact of the FMR1 gene on visual processing in fragile X syndrome. Brain 127, 591–601 (2004). [PubMed: 14736752]

11. Poort J et al. Learning Enhances Sensory and Multiple Non-sensory Representations in Primary Visual Cortex. Neuron 86, 1478–1490 (2015). [PubMed: 26051421]

12. Lee SH et al. Activation of specific interneurons improves V1 feature selectivity and visual perception. Nature 488, 379–383 (2012). [PubMed: 22878719]

13. Zupan B & Toth M Wild-type male offspring of fmr-1+/− mothers exhibit characteristics of the fragile X phenotype. Neuropsychopharmacology 33, 2667–2675 (2008). [PubMed: 18172434]

14. Zhang Y et al. Dendritic channelopathies contribute to neocortical and sensory hyperexcitability in Fmr1(-/y) mice. Nat Neurosci 17, 1701–1709 (2014). [PubMed: 25383903]

15. Arnett MT, Herman DH & McGee AW Deficits in tactile learning in a mouse model of fragile X syndrome. PLoS One 9, e109116 (2014). [PubMed: 25296296]

16. Juczewski K et al. Somatosensory map expansion and altered processing of tactile inputs in a mouse model of fragile X syndrome. Neurobiol Dis 96, 201–215 (2016). [PubMed: 27616423]

17. Goncalves JT, Anstey JE, Golshani P & Portera-Cailliau C Circuit level defects in the developing neocortex of Fragile X mice. Nat Neurosci 16, 903–909 (2013). [PubMed: 23727819]

18. La Fata G et al. FMRP regulates multipolar to bipolar transition affecting neuronal migration and cortical circuitry. Nat Neurosci 17, 1693–1700 (2014). [PubMed: 25402856]

19. Chen TW et al. Ultrasensitive fluorescent proteins for imaging neuronal activity. Nature 499, 295–300 (2013). [PubMed: 23868258]

20. Gonchar Y & Burkhalter A Three distinct families of GABAergic neurons in rat visual cortex. Cereb Cortex 7, 347–358 (1997). [PubMed: 9177765]

21. Zariwala HA et al. A Cre-Dependent GCaMP3 Reporter Mouse for Neuronal Imaging In Vivo. The Journal of neuroscience : the official journal of the Society for Neuroscience 32, 3131–3141 (2012). [PubMed: 22378886]

22. Hofer SB et al. Differential connectivity and response dynamics of excitatory and inhibitory neurons in visual cortex. Nat Neurosci 14, 1045–1052 (2011). [PubMed: 21765421]

23. Runyan CA & Sur M Response selectivity is correlated to dendritic structure in parvalbumin-expressing inhibitory neurons in visual cortex. J Neurosci 33, 11724–11733 (2013). [PubMed: 23843539]

24. Armbruster BN, Li X, Pausch MH, Herlitze S & Roth BL Evolving the lock to fit the key to create a family of G protein-coupled receptors potently activated by an inert ligand. Proceedings of the National Academy of Sciences of the United States of America 104, 5163–5168 (2007). [PubMed: 17360345]

25. Mullard A Fragile X disappointments upset autism ambitions. Nat Rev Drug Discov 14, 151–153 (2015). [PubMed: 25722228]

26. Atallah BV, Bruns W, Carandini M & Scanziani M Parvalbumin-expressing interneurons linearly transform cortical responses to visual stimuli. Neuron 73, 159–170 (2012). [PubMed: 22243754]

27. Kato HK, Asinof SK & Isaacson JS Network-Level Control of Frequency Tuning in Auditory Cortex. Neuron 95, 412–423 e414 (2017). [PubMed: 28689982]

28. Knoth IS, Vannasing P, Major P, Michaud JL & Lippe S Alterations of visual and auditory evoked potentials in fragile X syndrome. Int J Dev Neurosci 36, 90–97 (2014). [PubMed: 24875778]

29. LeBlanc JJ et al. Visual evoked potentials detect cortical processing deficits in Rett syndrome. Ann Neurol 78, 775–786 (2015). [PubMed: 26332183]

30. Niell CM & Stryker MP Modulation of visual responses by behavioral state in mouse visual cortex. Neuron 65, 472–479 (2010). [PubMed: 20188652]

31. Pakan JM et al. Behavioral-state modulation of inhibition is context-dependent and cell type specific in mouse visual cortex. Elife 5 (2016).

32. Dipoppa M et al. Vision and Locomotion Shape the Interactions between Neuron Types in Mouse Visual Cortex. Neuron 98, 602–615 e608 (2018). [PubMed: 29656873]

33. Guo ZV et al. Flow of cortical activity underlying a tactile decision in mice. Neuron 81, 179–194 (2014). [PubMed: 24361077]

34. Mostany R & Portera-Cailliau C A craniotomy surgery procedure for chronic brain imaging. J Vis Exp (2008).

35. Golshani P & Portera-Cailliau C In vivo 2-photon calcium imaging in layer 2/3 of mice. J Vis Exp (2008).

36. Pologruto TA, Sabatini BL & Svoboda K ScanImage: flexible software for operating laser scanning microscopes. Biomed Eng Online 2, 13 (2003). [PubMed: 12801419]

37. Mineault PJ, Tring E, Trachtenberg JT & Ringach DL Enhanced Spatial Resolution During Locomotion and Heightened Attention in Mouse Primary Visual Cortex. J Neurosci 36, 6382–6392 (2016). [PubMed: 27307228]

38. Cottam JC, Smith SL & Hausser M Target-specific effects of somatostatin-expressing interneurons on neocortical visual processing. J Neurosci 33, 19567–19578 (2013). [PubMed: 24336721]

39. Akerboom J et al. Optimization of a GCaMP calcium indicator for neural activity imaging. The Journal of neuroscience : the official journal of the Society for Neuroscience 32, 13819–13840 (2012). [PubMed: 23035093]

40. Hooper SR et al. Executive functions in young males with fragile X syndrome in comparison to mental age-matched controls: baseline findings from a longitudinal study. Neuropsychology 22, 36–47 (2008). [PubMed: 18211154]

41. Hamm JP, Peterka DS, Gogos JA & Yuste R Altered Cortical Ensembles in Mouse Models of Schizophrenia. Neuron 94, 153–167.e158 (2017). [PubMed: 28384469]

42. Pinto L & Dan Y Cell-Type-Specific Activity in Prefrontal Cortex during Goal-Directed Behavior. Neuron 87, 437–450 (2015). [PubMed: 26143660]

43. Harvey CD, Coen P & Tank DW Choice-specific sequences in parietal cortex during a virtual-navigation decision task. Nature 484, 62–68 (2012). [PubMed: 22419153]

44. Kogan CS et al. Integrative cortical dysfunction and pervasive motion perception deficit in fragile X syndrome. Neurology 63, 1634–1639 (2004). [PubMed: 15534248]

45. Plaisted K, O'Riordan M & Baron-Cohen S Enhanced visual search for a conjunctive target in autism: a research note. J Child Psychol Psychiatry 39, 777–783 (1998). [PubMed: 9690940]
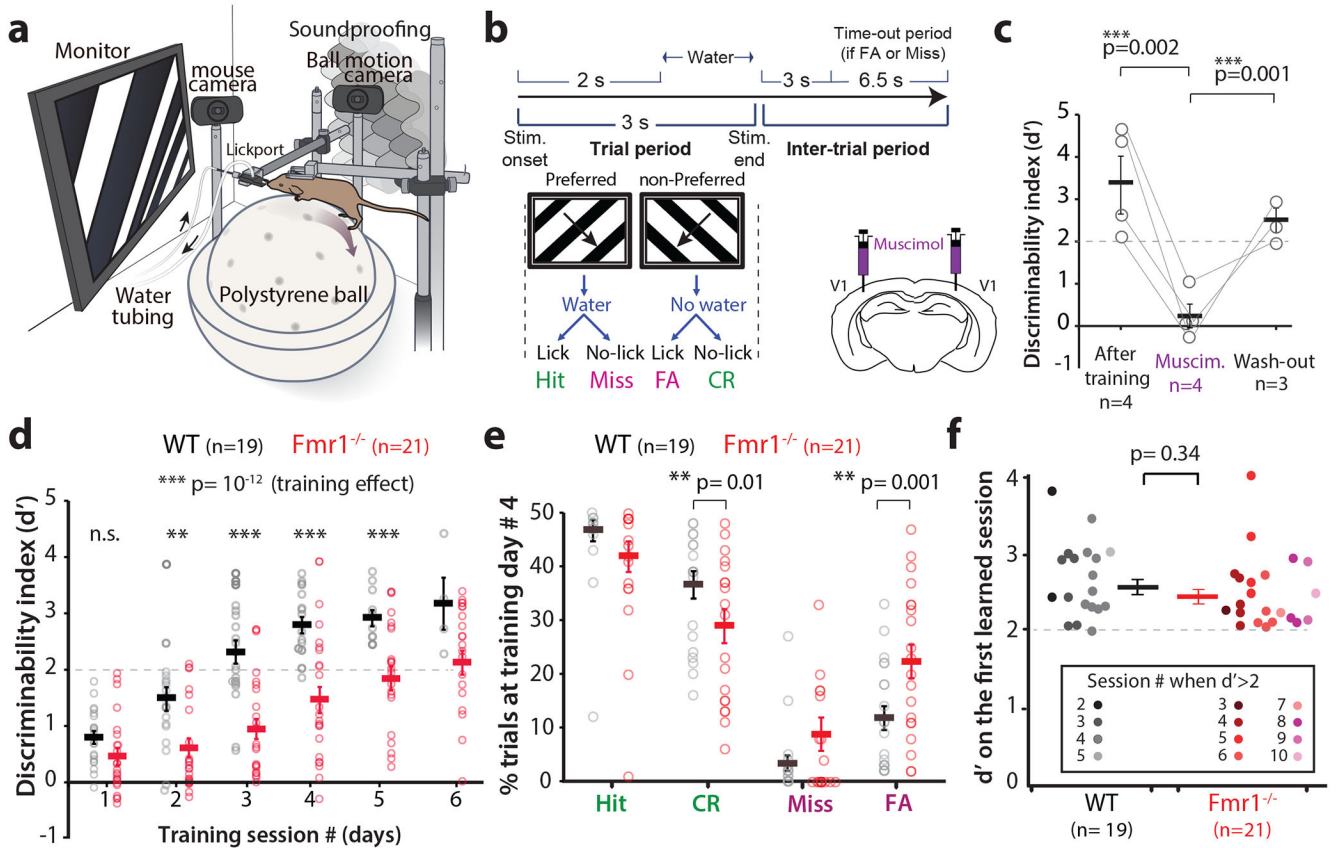
Figure 1: *Fmr1⁻/⁻* mice show delayed learning in a visual discrimination task.

a. Cartoon of the behavioral apparatus.

b. Timeline of an individual trial for the go/no-go visual discrimination task in water deprived mice. FA: false alarm; CR: correct rejection.

c. Bilateral inactivation of V1 with muscimol reversibly impairs task performance in expert WT mice, as measured by the discriminability index (d'). Repeated measures ANOVA., $F_{2,4}$ = 6.4, p=0.06. Unpaired one tailed Student's t-test, After Muscimol: p=0.002; After wash-out, p=0.001, In panels c-f horizontal bars indicate mean and error bars in this indicate the s.e.m. n=mice, indicated on the figure.

d. *Fmr1⁻/⁻* mice are delayed in learning of the basic task (90° difference between preferred and non-preferred stimuli). The dashed line at d'= 2 indicates expert performance threshold (equivalent to 90% correct rejections). Friedman test with repeated measures on training, followed by two-sided Mann-Whitney test for genotype effect at each session, $F_{4,185}$= 6.56, p= 0.2×10^{-12}. Session1: p= 0.065; Session 2: p= 0.008; Session 3: p= 0.7×10^{-4}; Session 4: p= 0.2×10^{-3}; Session 5: p= 0.003. n=mice, *Fmr1⁻/⁻* (21) and WT (19). *Fmr1⁻/⁻* mice took longer to achieve d>2. 3.5 ± 0.2 for WT vs. 6.0 ± 0.4 for *Fmr1⁻/⁻*; p= 7×10^{-6}, two-sided Mann-Whitney. * p<0.05; ** p<0.01

e. Lower task performance of *Fmr1⁻/⁻* mice on day #4 is associated with a significantly higher proportion of FA responses and lower proportion of CR responses. $11.3 \pm 2.2\%$ in WT vs. $22.3 \pm 3.1\%$ in *Fmr1⁻/⁻*; two-sided Mann-Whitney, p= 0.009.

f. There was no significant difference between genotypes in the d' on the first learned session (when mice reached d' 2). Unpaired, one-tailed Student t-test.
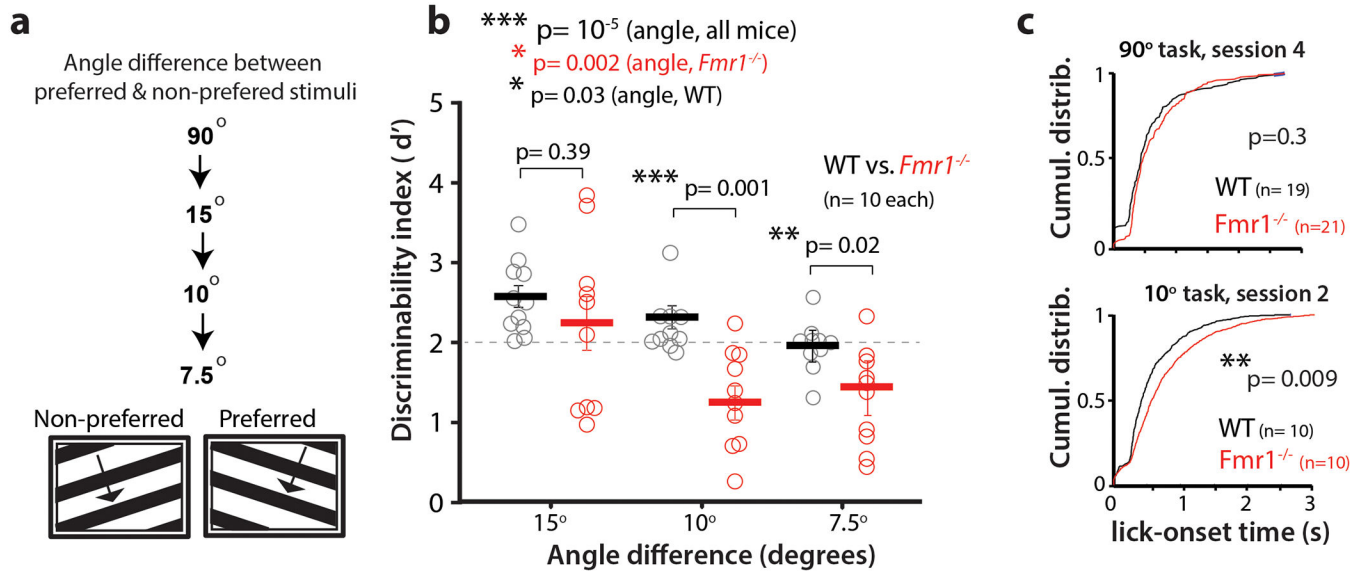
Figure 2: Reducing the angle between preferred and non-preferred stimuli impairs discrimination in *Fmr1*-/- mice

a. A reduced angle task was implemented after mice learned the 90° task (at 100% contrast, as in Fig. 1).

b. Selective impairment of *Fmr1*-/- mice in task performance at reduced angles between preferred and non-preferred stimuli. Friedman test (angle, all mice) $F_{2,57} = 1.96$, p= 6 × 10^{-5}. Two-sided Mann-Whitney (WT vs. Fmr1-/-), p values indicated on figure; Kruskal-Wallis (angle, each genotype) WT: $\chi^2_{2,28} = 12.66$, p= 0.002; *Fmr1*-/- : $\chi^2_{2,28} = 6.63$, p= 0.03. n= mice, Fmr1-/- (10), WT (10). Horizontal bars indicate mean and error bars indicate s.e.m.

c. *Fmr1*-/- mice show a significant delay in lick onset time on the reduced angle task (Hit trials) relative to WT mice. p= 0.009 Two- sided Kolmogorov-Smirnov test.
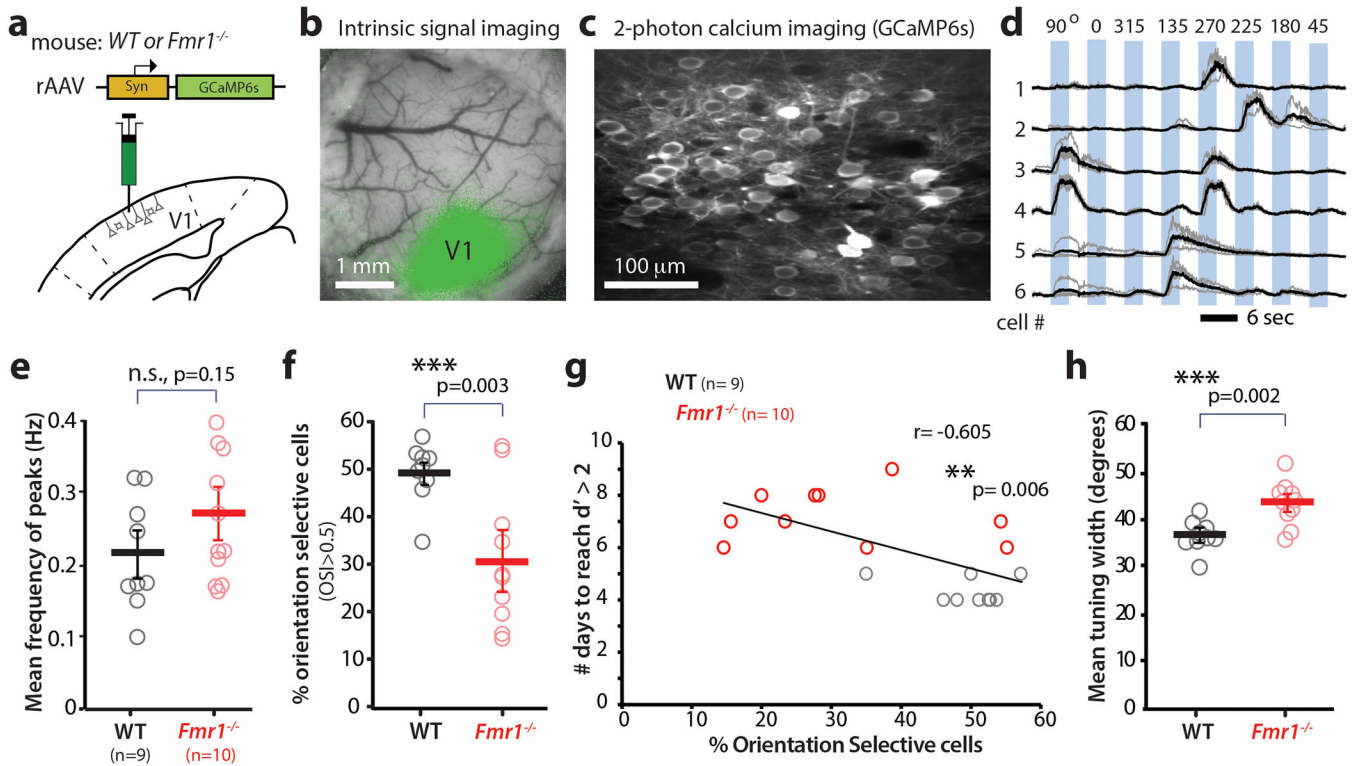
Figure 3: Orientation tuning deficits in V1 correlate with task performance in *Fmr1*^-/- mice.

>a. Cartoon of rAAV-GCaMP6s injection into V1.

b. Intrinsic signal imaging was then performed 2–3 weeks after rAAV injection to confirm appropriate targeting of V1 (green map).

c. Representative field of view for in vivo two-photon calcium imaging experiment in V1. Imaging was performed 3–4 weeks after rAAV injection at 15 fps.

d. Example traces of changes in GCaMP6s fluorescence intensity (F/F) for 6 representative neurons in V1 that exhibit a range of responses from narrow tuning (cell 1) to broad tuning (cells 2 & 3). Responses to single trials are shown in gray, averages of 4 responses are in black.

e. Visual evoked activity (as measured by the frequency of fluorescence peaks) is similar between WT and *Fmr1*^-/- mice. Unpaired, one-tailed Student t-test was used for panels e, f and h. The horizontal bars indicate mean and error bars indicate s.e.m. In panels e-h, n= mice, Fmr1^-/- (10), WT (9).

f. The percentage of orientation selective neurons in V1 is significantly lower in *Fmr1*^-/- mice. 49.5 ± 2.1% in WT vs. 31.2 ± 4.6% in *Fmr1*^-/-; p= 0.003, Unpaired two-tailed Student's t-test. Results showing a reduction in percentage of orientation selective pyramidal cells and increase in tuning width was replicated in 3 additional *Fmr1*^-/- mice (data shown in Fig 5h and i is comparable to Fig 3f and h.

g. Inverse correlation between the percentage of orientation selective neurons in V1 and performance on the visual discrimination task (as measured by the number of days required to reach a d'>2). r= −0.605, p= 0.006, Pearson's Correlation.

h. The mean orientation tuning width for V1 neurons is significantly higher in *Fmr1*^{-/-} mice. 36.7 ± 1.0° in WT vs. 43.3 ± 1.4° in *Fmr1*^{-/-}; p= 0.002, Unpaired two-tailed Student's t-test Tuning width also correlates with task performance (see Supplementary Fig. 7)
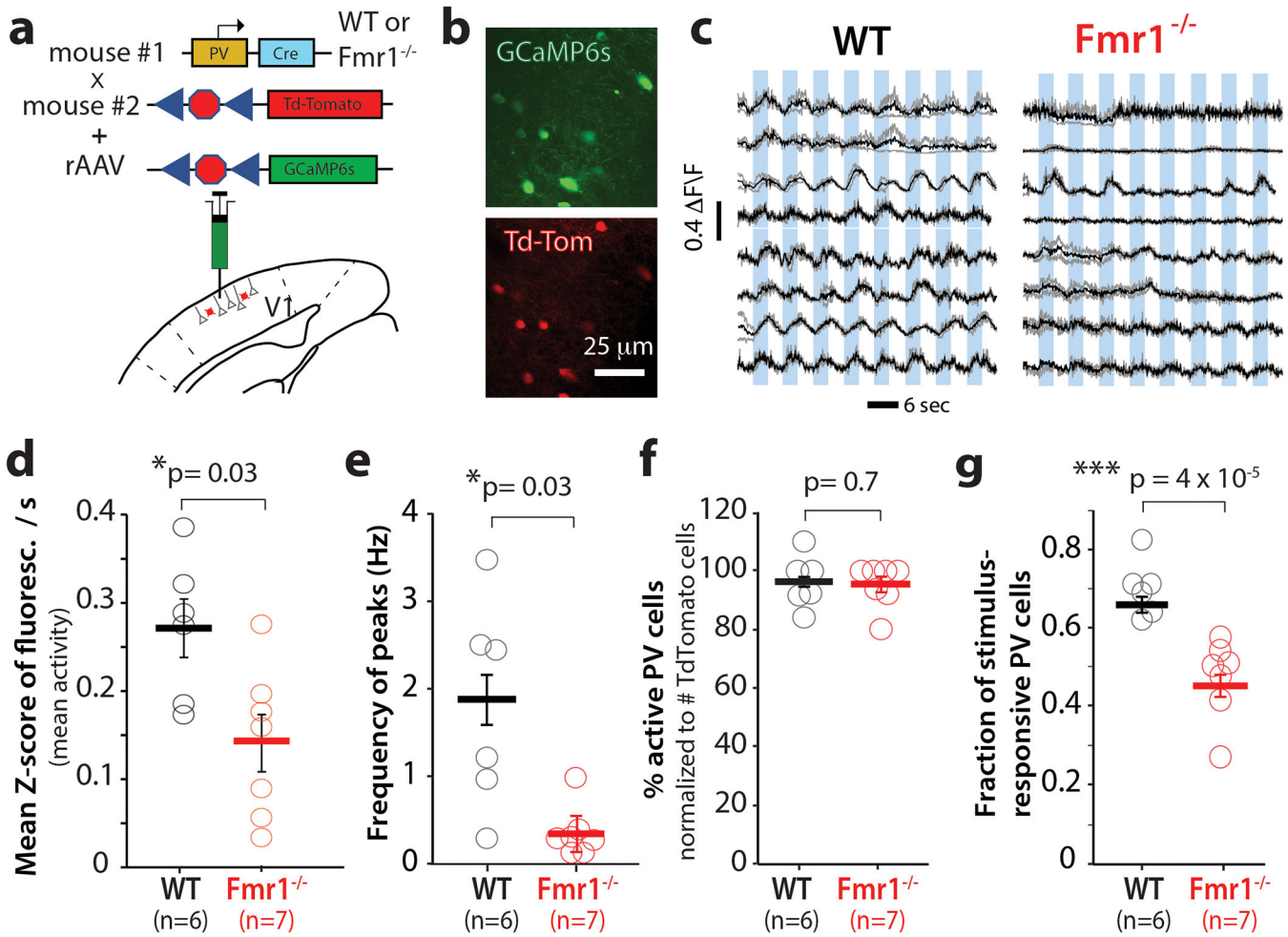
Figure 4: Parvalbumin interneurons in V1 in *Fmr1^-/-^* mice show reduced visual evoked activity.

a. Cartoon of strategy for selective GCaMP6s expression in PV interneurons.

b. Representative field of view for in vivo 2-photon calcium imaging in PV neurons expressing GCaMP6s (green) and Td-Tom (red).

c. Example traces of changes in GCaMP6s fluorescence intensity (F/F) for 8 representative PV neurons in V1 from 4 WT (left) and 4 *Fmr1^-/-^* mice (right). Responses to 8 different directions from single trials are shown in gray, while the averages of 4 trials are in black.

d. The overall frequency of visual evoked calcium transients (as measured by the mean fluorescence Z-scores per s) is significantly lower in *Fmr1^-/-^* mice. The horizontal bars indicate mean and error bars indicate s.e.m. n= mice, Fmr1^-/-^ (7), WT (6). 0.27 ± 0.06 for WT vs. 0.15 ± 0.03 for *Fmr1^-/-^*; p= 0.03. two- tailed Mann-Whitney test for panels d-f.

e. The frequency of visually evoked peaks of activity in PV neurons is significantly lower in *Fmr1^-/-^* mice. 1.8 ± 0.5 for WT vs. 0.3 ± 0.1 for *Fmr1^-/-^*; p= 0.03.

f. WT and *Fmr1^-/-^* mice and similar percentages of PV cells that were active, p= 0.70.

g. The fraction of visually responsive PV cells is significantly reduced in *Fmr1^-/-^* mice. 0.7 ± 0.02 for WT vs. 0.4 ± 0.03 for *Fmr1^-/-^*; $p < 10^{-5}$, Unpaired two-tailed Student's t-test. Note that there is an inverse correlation between the fraction of stimulus-responsive PV cells and behavioral performance (see Fig. 5i). Results showing a decrease in mean Z-score/sec

and fraction of stimulus responsive PV cells in *Fmr1*^{-/-} was independently replicated in Fig 5 (see data from *Fmr1*^{-/-} mice before CNO treatment in Fig 5c, d and e).
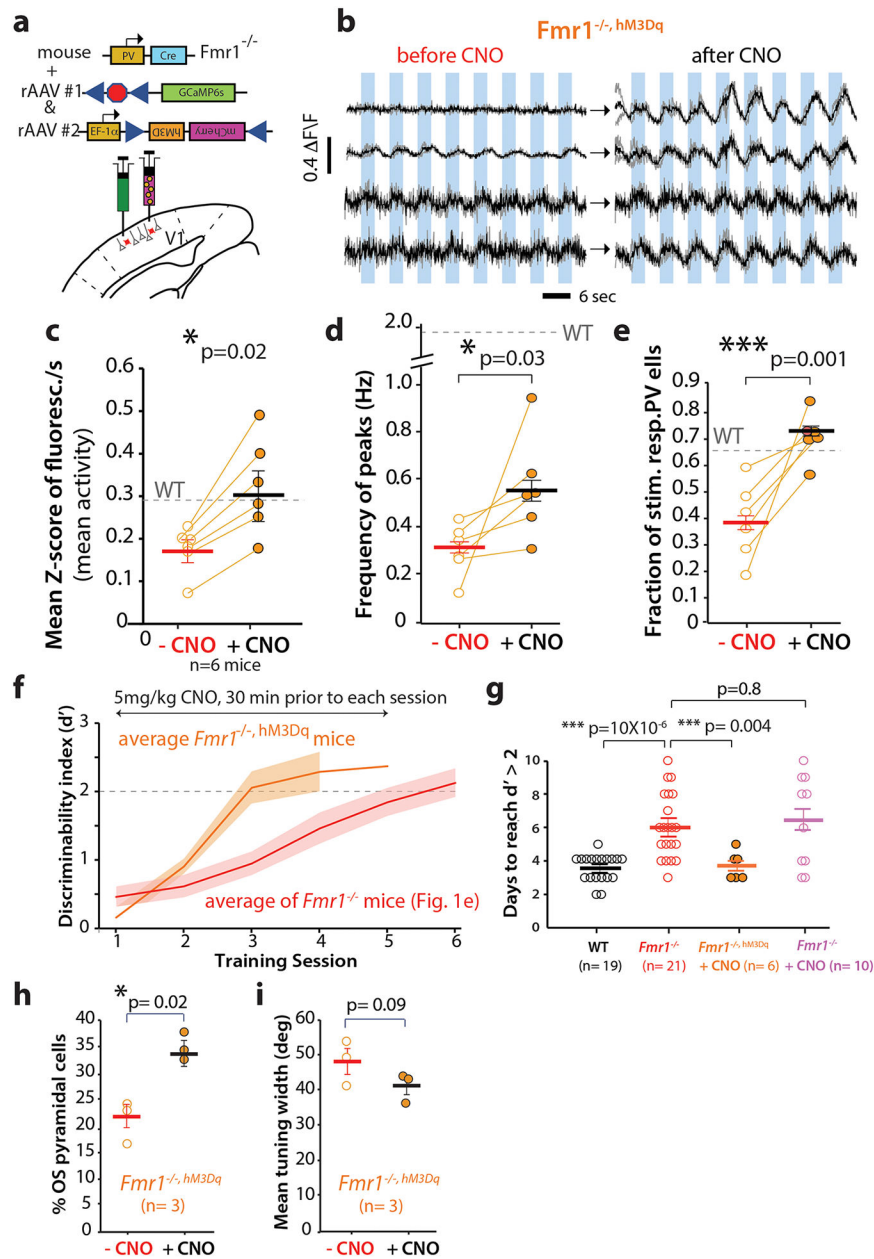
Figure 5: A DREADD strategy that restores normal PV cell activity in V1 rescues delayed learning in *Fmr1-/-* mice.

a. Cartoon of strategy for selective rAAV-EF1a-DIO-hM3D(Gq)-mCherry expression in PV interneurons of *Fmr1-/-* mice.

b. Example of GCaMP6s traces for 4 representative PV neurons in V1 from 4 different *Fmr1-/-, hM3Dq* mice before and ~30min after i.p. injection of clozapine N-oxide (CNO).

c, d. The activity of PV cells, as measured by both mean fluorescence Z-score/sec (**c**: 0.20 ± 0.02 Z-score/sec before CNO vs. 0.32 ± 0.05 Z-score/s after CNO; p= 0.02) or the frequency of peaks in calcium transients (**d**: 0.3 ± 0.04 Hz before CNO vs. 0.6 ± 0.1 Hz after CNO; p= 0.03), in *Fmr1-/-, HM3Dq* mice increases significantly after CNO administration. For all panels the horizontal bars indicate mean and error bars indicate s.e.m. n= mice,

Fmr1$^{-/-}$ (6, before and after CNO). A one-tailed, unpaired Student t-test was used for panels c-e and h-i.

e. The fraction of stimulus-responsive PV cells also increases significantly after CNO. 0.4 ± 0.06 before CNO vs. 0.7 ± 0.04 after CNO; p= 0.001. Note that the fraction of visually responsive PV cells was comparable between *Fmr1*$^{-/-}$ mice expressing DREADDs (before CNO) and *Fmr1*$^{-/-}$ mice in Fig. 4g.

f. *Fmr1*$^{-/-, HM3Dq}$ mice treated with CNO 30 min prior to each session learned the basic 90° task in ~3 d on average. The rate of learning for *Fmr1*$^{-/-}$ mice (from Fig. 1d) is shown for comparison. The solid line indicates the mean, and the shaded area shows the standard error. The dashed line at d'= 2 indicates expert performance threshold.

g. *Fmr1*$^{-/-, HM3Dq}$ mice treated with CNO learned the basic 90° task significantly faster than *Fmr1*$^{-/-}$ mice and as fast as WT mice. WT: 3.5 ± 0.2 d, *Fmr1*$^{-/-}$: 6.0 ± 0.4 d; *Fmr1*$^{-/-, hM3Dq}$ with CNO: 3.7 ± 0.3 d; *Fmr1*$^{-/-}$ with CNO: 6.4 ± 0.8 d; $\chi^2_{3,55}$, p= 5 X 10^{-5}, Kruskal-wallis test; WT vs. *Fmr1*$^{-/-}$: p=10×10^{-6} two-tailed Mann-Whitney test; *Fmr1*$^{-/-}$ vs. *Fmr1*$^{-/-, hM3Dq}$ with CNO: p= 0.004; two-sided Mann-Whitney test. In a control experiment, treating Fmr1$^{-/-}$ mice (without DREADD) with CNO had no effect on the time to learn the task, p= 0.8, two-tailed Mann-Whitney test. n=mice, WT(19), *Fmr1*$^{-/-}$(21), *Fmr1*$^{-/-, HM3Dq}$+CNO(6), *Fmr1*$^{-/-}$+CNO(10).

h. The percentage of OS pyramidal neurons in *Fmr1*$^{-/-, HM3Dq}$ mice was significantly higher after CNO administration, p= 0.02, Unpaired one-tailed Student's t-test. *Fmr1*$^{-/-, HM3Dq}$(same mice were tested before and after CNO, n=3)

i. There was a non-significant trend toward reduced tuning width of pyramidal neurons in *Fmr1*$^{-/-, HM3Dq}$ mice after CNO administration, p= 0.09, Unpaired one-tailed Student's t-test. *Fmr1*$^{-/-, HM3Dq}$(before and after CNO same mice, n=3)
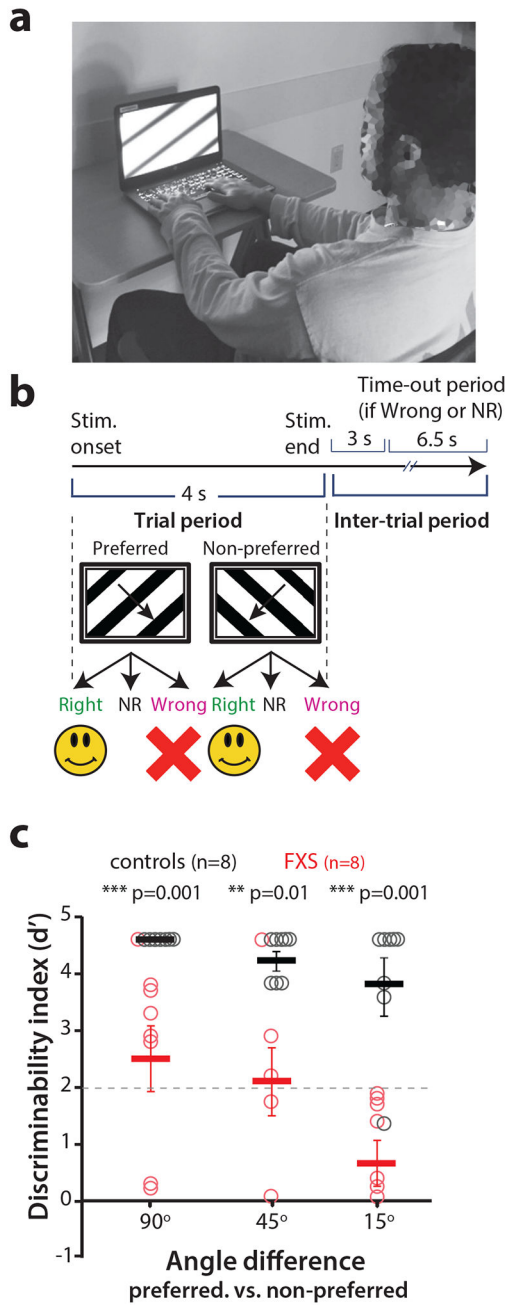
Figure 6: Fragile X patients exhibit similar defects in visual discrimination as *Fmr1*$^{-/-}$ mice

a. Photograph of a FXS subject performing the visual discrimination task.

b. Timeline of an individual trial for the visual discrimination task in human subjects. NR: no response.

c. Task performance at different angles between preferred and non-preferred orientation stimuli for FXS subjects and age-matched control participants. Individuals with FXS are able to perform the 90° visual discrimination task with d'> 2 but they exhibited a significantly lower d' than controls with the reduced angle task. 90°: p= 0.001; 45°: p= 0.01; 15°: p= 0.001, two-tailed Mann-Whitney test for FXS vs. controls at different angles.

Kruskal-wallis test for comparisons across all angles, p=0.06. The horizontal bars indicate mean and error bars indicate s.e.m. n= human subjects, FXS (8), Controls (8).